






Packaged Multi-Core Fiber Interferometer for High-Temperature Sensing

Josu Amorebieta , Gaizka Durana , Angel Ortega-Gomez , Rubén Fernández, Javier Velasco, Idurre Sáez de Ocáriz, Joseba Zubia , Jose Enrique Antonio-López, Axel Schülzgen , *Fellow, OSA*, Rodrigo Amezcua-Correa, and Joel Villatoro

Abstract—A small size and compactly packaged optical sensor for high-temperature measurements is reported. The sensor consists of a short piece of multi-core fiber (MCF) spliced to the distal end of a single-mode fiber. The packaging consists of an inner ceramic shield that prevents bending, curvature, and vibration effects on the MCF, and an outer metallic shield that protects the device against impacts. The interaction between specific supermodes excited in the MCF creates an interference pattern that shifts linearly with the temperature. The sensor was calibrated in the range from 200 to 1000 °C and a K-type thermocouple was used as a reference. The average temperature sensitivity was found to be 24.8 pm/°C with a response time of 15 s. Our results indicate that our MCF interferometric thermometer is as accurate as an electronic one with the advantage that it is passive. Therefore, we believe that the proposed sensor is suitable for industrial applications.

Index Terms—High temperature measurement, mode interferometers, multi-core fibers, optical sensors, optical thermometers, supermodes.

I. INTRODUCTION

IN THE industrial sector, there are several environments and applications where high temperature is present. For example, in engine tests, metallurgical processes, in gas and oil facilities, etc. In such harsh environments, temperature can reach very

high values (up to 1000 °C, and even higher). Thus, accurate measurement of temperature is crucial.

Currently, the technology commonly accepted and well established for high temperature measurement is based on thermocouples [1]–[5]. However, due to their electronic nature, thermocouples may not be a viable solution for applications or environments where electromagnetic or microwave radiation is present. In such cases, optical fiber thermometers are a good alternative since they are totally passive.

Optical fibers exhibit an intrinsic sensitivity to temperature, which makes them ideal for temperature sensing. In fact, throughout the years, many different optical fiber temperature sensors have been demonstrated [6]–[10]. Most optical fiber thermometers operate in a limited temperature range. However, the use of specialty optical fibers and innovative approaches and techniques have allowed expanding the temperature range up to 1000 °C. Thus, optical fiber thermometers may reach the performance and capabilities of thermocouples and be a real alternative for high temperature sensing, hence for industrial applications.

The most common approach for high temperature sensing consists of using regenerated fiber Bragg gratings (rFBGs), also called chemical composition gratings [11]–[14]. The operating principle of such sensors is based on the thermo-optic effect that modifies the period of the grating. rFBG-based sensors have temperature sensitivity of around 10 pm/°C, and their response time is of several seconds [15]–[18]. The disadvantage of rFBGs sensors is their high cost, as their fabrication and interrogation require expensive setups, lasers, and picometer-resolution detectors.

Fabry-Perot interferometry has been widely studied for high temperature sensing as well. In this technique, the sensitive element is a cavity that can be fabricated from temperature-resistant materials such as pure glass or sapphire [19]–[24]. The advantages of the Fabry-Perot interferometers (FPI) include high sensitivity and small size. However, their performance is directly linked to the uniformity of the cavity, which is not easy to achieve.

Other alternatives for high temperature sensing are based on long period gratings (LPGs) [25]–[27] and different types of interferometers [28]–[31]. The drawback of LPGs is their sensitivity to the surrounding medium, which imposes proper isolation to measure temperature only. On the other hand, most interferometers provide relative temperature measurements, as they are

Manuscript received November 20, 2018; revised January 16, 2019 and February 20, 2019; accepted February 27, 2019. Date of publication March 7, 2019; date of current version April 17, 2019. This work was supported in part by the Fondo Europeo de Desarrollo Regional, in part by the Ministerio de Economía y Competitividad under Project TEC2015-638263-C03-1-R, and in part by the Gobierno Vasco/Eusko Jaurlaritza IT933-16 and ELKARTEK (KK/00033, KK-2017/00089, and KK-2018/00078). The work of J. Amorebieta was supported in part by a Ph.D. fellowship from the University of the Basque Country UPV/EHU, Vicerrectorado de Euskera y Formación Continua. (*Corresponding author: Josu Amorebieta.*)

J. Amorebieta, G. Durana, A. Ortega-Gomez, R. Fernández, and J. Zubia are with the Department of Communications Engineering, University of the Basque Country, E-48013 Bilbao, Spain (e-mail: josu.amorebieta@ehu.eus; gaizka.durana@ehu.eus; angel.ortega@ehu.eus; ruben.fernandez@ehu.eus; joseba.zubia@ehu.eus).

J. Velasco and I. Sáez de Ocáriz are with the Science and Technology Department, Fundación Centro de Tecnologías Aeronáuticas, E-01510 Miñano Mayor, Spain (e-mail: javier.velasco@ctaero.com; idurre.saezdeocariz@ctaero.com).

J. E. Antonio-López, A. Schülzgen, and R. Amezcua-Correa are with the CREOL, The College of Optics and Photonics, University of Central Florida, Orlando, FL 32816 USA (e-mail: jealopez@creol.ucf.edu; axel@creol.ucf.edu; r.amezcua@creol.ucf.edu).

J. Villatoro is with the Department of Communications Engineering, University of the Basque Country, E-48013 Bilbao, Spain, and also with the IKERBASQUE-Basque Foundation for Science, E-48013 Bilbao, Spain (e-mail: agustinjoel.villatoro@ehu.eus).

Color versions of one or more of the figures in this paper are available online at <http://ieeexplore.ieee.org>.

Digital Object Identifier 10.1109/JLT.2019.2903595

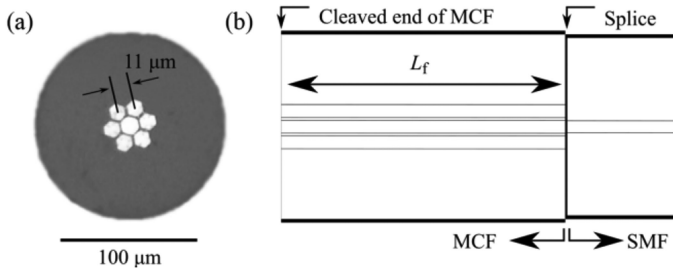


Fig. 1. (a) Picture of the cross-section of the MCF used to build the temperature sensor. (b) Schematic representation of the sensor architecture. L_f is the length of the MCF. The cleaved end reflects less than the 4% of the emitted light.

codified in the shift of interference patterns. As a result, LPG- and interferometer- based high temperature sensors have not reached the market yet.

As an alternative to the existing optical fiber thermometers for high temperature, in this work, we propose a sensor that may overcome the main limitations and drawbacks mentioned above. Our device consists of a short segment of MCF spliced to the distal end of a typical SMF. The fabrication of our device is easy, reproducible, and inexpensive. The temperature sensitive region of our device is the segment of MCF that can withstand high temperatures (up to 1000 °C) as demonstrated in [32]–[34]. In our case, the sensor operates in reflection mode. In addition, we have packaged our device with a double shielding (ceramic and metallic). The packaging eliminates the effects of strain, bending, curvature, or vibrations on the MCF interferometer as it is sensitive to such parameters [35]–[38].

The reflection spectrum of our device is sinusoidal and shifts when temperature changes. The interference pattern of our MCF sensor is easily traceable, thus, it is easy to establish a relationship between the absolute maximum of the interference pattern and temperature. With our packaged MCF sensor, temperatures up to 1000 °C, response times at different temperature gradients and its robustness against vibrations were measured. For comparison, similar experiments were also carried out with a bare MCF interferometer. The results suggest that the proposed packaging does not compromise the temperature sensitivity of our device. In addition, our packaged sensor is as accurate as a K-type thermocouple, which is widely used and accepted as reference in the industry.

II. OPERATION PRINCIPLE, DESIGN AND FABRICATION

In the device reported here, the MCF is the key element. The MCF, fabricated at the University of Central Florida (Orlando, USA), has a particular structure based on seven identical hexagonal cores. Six of them are concentrically arranged in a ring-like shape around a central one. The mean diameter and distance among adjacent axes is 9.2 μm and 11 μm, respectively, see Fig. 1(a). All the cores are made of germanium doped silica glass and are inlaid in pure silica cladding. The numerical aperture (NA) of each core is 0.14 at 1550 nm that is the same NA of a typical SMF. The outer diameter of the fiber is 130 μm.

A scheme of the MCF interferometer is shown in Fig. 1(b). The device consists of a short MCF segment fusion spliced to a

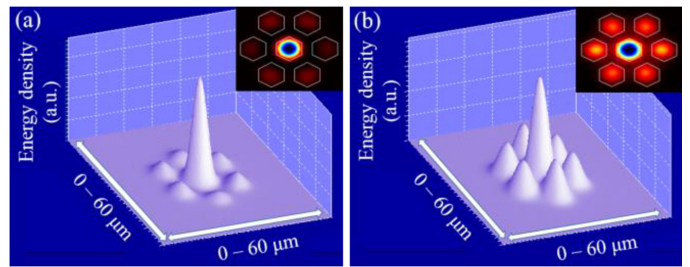


Fig. 2. Simulations of the 3D and 2D profiles of the two supermodes excited in the MCF. In (a) the supermode SP_{01} is shown, and in (b) the supermode SP_{02} . The inset 2D profiles have an area of $60 \times 60 \mu\text{m}^2$.

conventional SMF. A fiber fusion splicer (Fujikura 100 P+) was used to fabricate the device. Such a machine aligns precisely the single core of the SMF with the central core of the MCF. Due to that, the insertion loss of supermode interferometers is minimal (typically 0.1 dB or below) as reported in [35].

The MCF described above is called strongly-coupled multi-core fiber, which means its cores are close enough to each other to allow interaction among them. The modes supported by such an MCF are called supermodes [39], [40], which are the linear combination of individual LP modes of each core of the MCF. In our device, schematically shown in Fig. 1(b), the excitation of the MCF is with the LP_{01} (fundamental) mode of the SMF. This, combined with the axial symmetry of the SMF-MCF structure, causes only two specific supermodes to be excited in the MCF. The profiles of such supermodes are shown in Fig. 2.

The effective refractive index of each supermode is different, thus, a phase difference between them can be expected as they propagate through the length of the MCF (L_f). The phase difference ($\Delta\varphi$) will be $\Delta\varphi = 4\pi\Delta nL_f/\lambda$, where $\Delta n = n_2 - n_1$, with n_1 and n_2 being the indices of the supermodes SP_{01} and SP_{02} , respectively, and λ the wavelength of the light source. According to our simulations, the value of Δn was 7.8×10^{-4} at $\lambda = 1545$ nm. The phase difference will cause a coupling between both supermodes, which will generate a sequence of maximum and minimum values in the reflection spectrum of our MCF interferometer. When the reflection reaches a maximum value to a given wavelength, the interference is constructive, which means that the two supermodes are in phase and, therefore, their coupled power is maximum for that wavelength. The maximum values appear when the phase difference equals an integer multiple of 2π ($m2\pi$, where $m = 1, 2, 3 \dots$). Thus, by considering that the reflected light travels twice the length of the MCF ($2L_f$), the maxima are located at the following wavelengths:

$$\lambda_m = 2L_f\Delta n/m. \quad (1)$$

In general, in an optical fiber, the thermo-optic effect prevails over the thermal expansion effect. Thus, for temperature measurements, only the changes in the refractive index of the fiber core (or cores) are considered [28], [32]. In our case, such changes induce a variation in the effective indices of the interfering supermodes, and hence, a shift in the interference pattern. Therefore, by monitoring λ_m , the temperature around the MCF can be known. It is important to point out that with our MCF

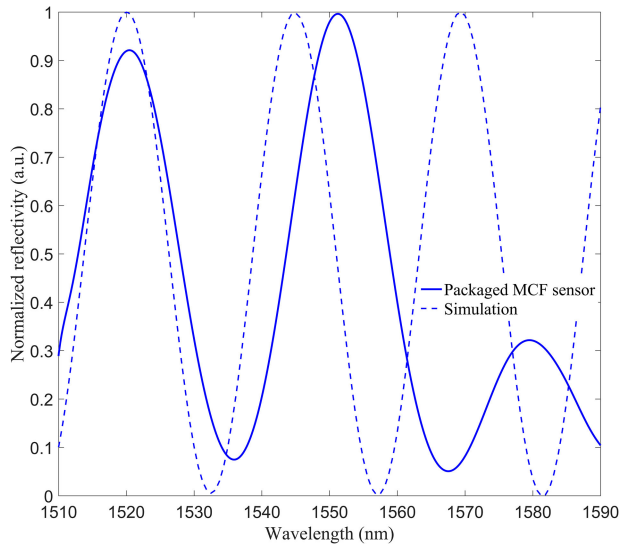


Fig. 3. Interference pattern obtained by simulation for a 2.54 cm-long MCF interferometer (dashed line) and with the fabricated device (solid line).

interferometer the measurement of temperature is absolute, as it will be codified in wavelength.

In order to measure the widest temperature range possible, the length of the MCF segment is crucial. On the one hand, the displacement of λ_m , which shifts around $30 \text{ pm}/^\circ\text{C}$ without any packaging [32], must not overlap with the maximum located at λ_{m+1} or λ_{m-1} . On the other hand, λ_m must be within the wavelength range of the sensor interrogator, which in our case was between 1510 and 1595 nm, at any temperature of the measuring range. Thus, to achieve the aforementioned requirements, two different simulation programs (Matlab MathWorks and Photon-Design) were used in which Eq. (1) was implemented with the parameters of the MCF and the desired initial position of λ_m established to obtain the MCF length. It was calculated to be 2.545 cm. However, due to the difficulty for obtaining an MCF segment of that precision with a conventional cleaver, we fabricated a device with $L_f = 2.54 \text{ cm}$ with an error of approximately $200 \mu\text{m}$.

Fig. 3 shows the spectra of the designed and fabricated interferometers at room temperature. For the calculated MCF length, the difference between the maxima and minima (visibility) is of 0.9. The difference between the simulated and observed pattern is due to the impossibility of reproducing the ideal conditions of the simulation in real-life conditions, such as the fact that the simulation programs use a flat spectrum light source whereas the manufactured sensor uses a Gaussian-like emission light source. It can be noted that the peak at which simulated and manufactured sensor's patterns match is located at 1520 nm. As temperature increases, such a peak is expected to shift to longer wavelengths [32]. Hence, the peak located at 1520 nm (λ_m) was selected to be monitored and correlated with temperature.

In order to make the MCF interferometer sensitive exclusively to temperature, it was packaged as follows: The bare SMF-MCF structure, whose total length was approximately 15 cm, was protected with a double shielding. The first layer was a double bore thin ceramic tube (Omega Engineering TRX-005132-6). Each

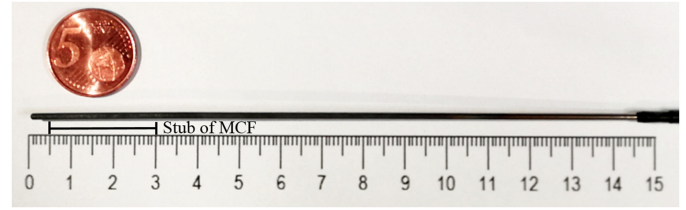


Fig. 4. Picture of the manufactured MCF sensor after being exposed to 1000°C . Notice that the metallic tube has a blackening gradient that indicates the different temperatures on the tube. The position and length (2.54 cm) of the MCF segment are indicated. The gap between the tip of the metallic tube and the stub of MCF is long enough to avoid a Fabry-Perot cavity.

bore had a diameter of $127 \mu\text{m} \pm 5\%$. In this manner, the MCF and part of the SMF were kept straight. Thus, bending effects on the interference pattern of the MCF were eliminated. The second layer was a stainless steel tube (Omega Engineering SS-116-6CLOSED) that covered the ceramic layer and provided physical protection against possible impact or shocks. A photograph of the final sensor prototype is shown in Fig. 4. As it can be noticed, the sensitive part of the sensor is only 2.54 cm long and located at the edge of the shielding. Thus, the sensor could be just about 3 cm long. The reason for the extra 12 cm is to protect the SMF due to the configuration of the furnace. The latter had a circular hole (slightly bigger than the sensor in diameter) that only in the deepest part reached temperatures of 1000°C . This causes that the packaged sensor has to be vertically inserted completely. As it can be seen in the blackening gradient in Fig. 4, the area where the MCF is located is the area that has been exposed to the highest temperatures.

The interrogation of our MCF interferometer consisted of a broadband light source centered at 1550 nm, with Gaussian-like emission, a 50:50 coupler and a small spectrum analyser (I-MON512-USB, Ibsen Photonics). The data processing was made with an *ad hoc* program developed in Matlab MathWorks. The data processing approach was as follows: Raw spectra provided by the spectrum analyser were collected at different temperatures; then, the spectra were averaged and normalized. After that, a Savitzky-Golay filter was applied to every spectra in order to smooth them. Finally, the highest peak (λ_m), or absolute maximum of the interference pattern, was found. The wavelength at which the maximum was located was correlated with temperature, which was measured with a K-type thermocouple used for temperature calibration measurements (Herten, K-type, SN TCP187).

III. RESULTS AND DISCUSSION

The tests were performed at the Aeronautical Technologies Centre (CTA) facilities located in the Alava Technology Park (Spain). The heating/cooling processes were carried out with a programmable high temperature furnace (Isotech Pegasus Plus 1200). Before running the calibration measurements, a curing process was carried out to eliminate as much as possible the hysteresis effect of the sensor [28]. The calibration was performed repeatedly in the range from 200 to 1000°C , in steps of 50°C that lasted 70 minutes each. Thus, overall, each calibration lasted 100 hours approximately. The sampling rate was 1 Hz.

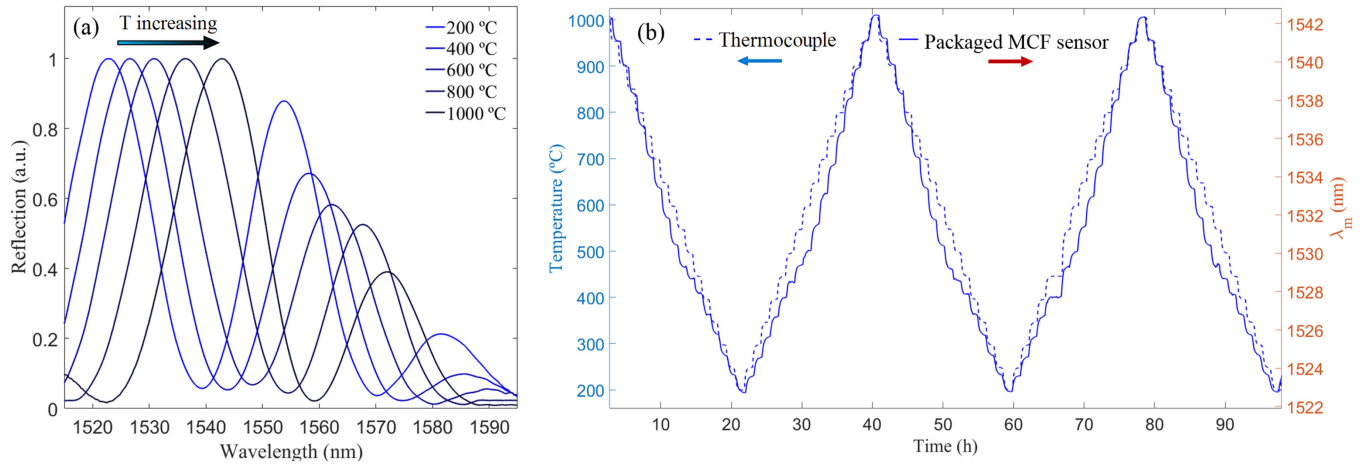


Fig. 5. (a) Spectra observed in the 200-1000 °C temperature range. (b) Time evolution of our packaged MCF sensor compared to that of the thermocouple. Colored arrows indicate the corresponding vertical axis of each curve.

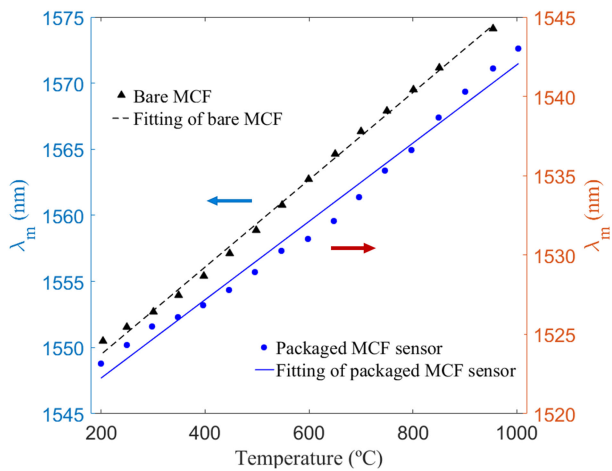


Fig. 6. Calibration curve of the packaged MCF sensor (solid dots, solid line) and 2.54 cm of bare MCF (triangles, dashed line). Colored arrows indicate the corresponding axis of each curve.

Fig. 5(a) shows the reflection spectra of our packaged MCF interferometer at different temperatures. It can be seen that the shift for the thermal range under study was around 20 nm. The position of the maximum peak as a function of time is shown in Fig. 5(b). For comparison, the time evolution of the temperature measurement provided by the thermocouple is also shown. From the monitored λ_m and temperature data, the calibration curve of the packaged MCF sensor was obtained, which is shown in Fig. 6. In order to evaluate the effect of the shielding on the temperature sensitivity of the packaged MCF sensor, the calibration curve obtained from a 2.54 cm-long bare MCF device that was subjected to an identical calibration process as the packaged MCF sensor is also shown in Fig. 6.

For the packaged MCF sensor, the Pearson squared correlation coefficient was found to be $R^2 = 0.9856$ and the uncertainty of $\sigma^2 = 0.611 \text{ nm}^2$ [41]. The correlation between temperature (in °C) and λ_m (in nm) that was obtained from the experiments was:

$$T = 39.929\lambda_m - 60525. \quad (2)$$

This indicates that the temperature sensitivity of the packaged MCF sensor was 24.8 pm/°C. From the calibration curve of the 2.54 cm-long bare MCF sensor shown in Fig. 6, we obtained a temperature sensitivity of 31.47 pm/°C. The latter agrees with that (29 pm/°C) of the MCF thermometer reported in [32] in the range between 100°C and 300°C, which was fabricated with bare MCF as well. Therefore, the packaging proposed here does not compromise the temperature sensitivity of the device. As a matter of fact, the main purpose of protecting the SMF and the MCF with a close-fitting ceramic tube was to keep the fibers tightly in the axial direction so that the measurements were strictly related to temperature and not affected by undesired effects of bending or vibrations, something that cannot be achieved when unprotected MCF is used. This may be the cause of the performance differences between the packaged MCF sensor and the bare MCF shown in Fig. 6 and the one reported in [32] where non-linear response to temperature was observed.

The response and recovery times of our packaged MCF temperature sensor and those of the device built with bare MCF were also evaluated as these are important parameters to be considered. The rising and falling times were measured several times at different temperature gradients. The measurements were carried out for 2 different thermal loops: from 25 °C to 550 °C, and back to 25 °C, and from 25 °C to 900 °C, and back to 25 °C. In each case, the response time of both optical devices and that of the K-type thermocouple were recorded. The response time ($\tau_{63\%}$), or time constant, is defined as the time required to reach 63.2% of an instantaneous change in temperature [42].

The results for the 25 °C–550 °C–25 °C loop are shown in Fig. 7. The results shown in Fig. 7 indicate that the shift of λ_m of the bare MCF device was more than expected according to the sensitivity obtained from its calibration curve shown in Fig. 6. This means that the shift of λ_m may not be strictly due to temperature as the MCF segment was also exposed to bending and/or vibrations induced by the furnace. The tracked peak of the packaged MCF sensor shifts 10.1 nm and shows a smoother and less noisy curve compared to that of the bare MCF. This shift agrees with the combination of the sensitivity of the sensor in

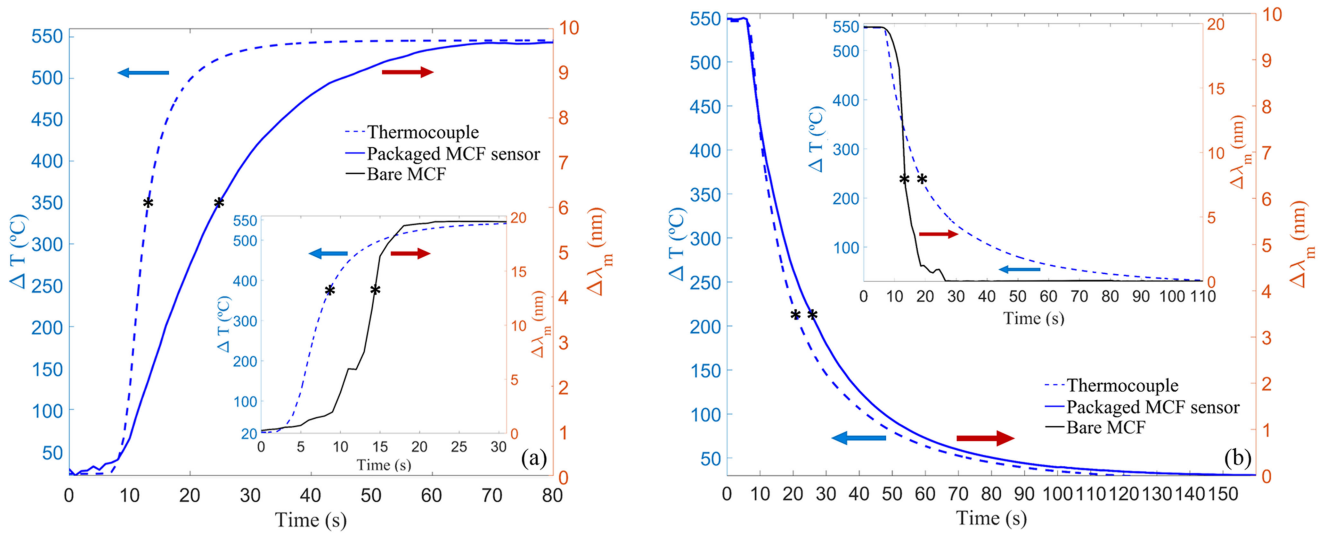


Fig. 7. Response times for (a) heating from 25 °C to 550 °C and for (b) cooling from 550 °C to 25 °C of a packaged and bare MCF sensors. For comparison, the response and recovering times of a commercial thermocouple are shown. Notice the non-uniform shape of the curves of the bare MCF compared to that of the packaged MCF. Colored arrows indicate the corresponding vertical axis of each curve. The black asterisk (*) in each curve represents the $\tau_{63\%}$ of each sensor.

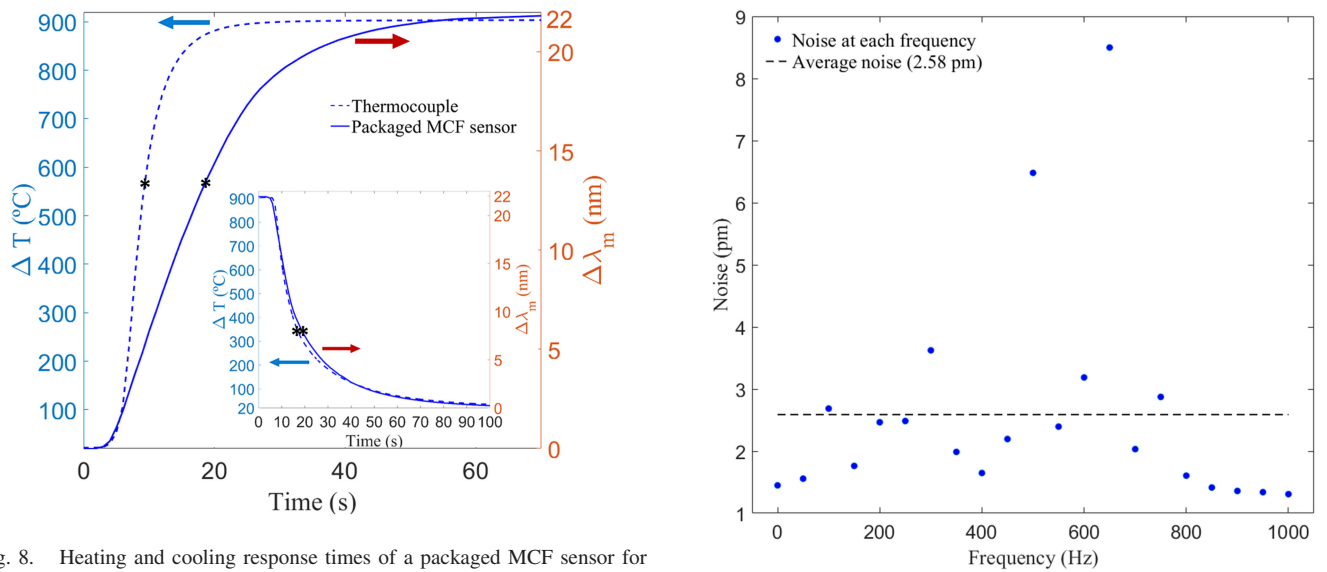


Fig. 8. Heating and cooling response times of a packaged MCF sensor for the 25 °C-900 °C-25 °C loop. Colored arrows indicate the corresponding axis of each curve. The black asterisk (*) in each curve represents the $\tau_{63\%}$ of each sensor.

TABLE I
RESPONSE TIMES (IN S) OF THE PACKAGED MCF SENSOR AND THE THERMOCOUPLE

Temperature gradient (°C)	25 - 550	550 - 25	25 - 900	900 - 25
Thermocouple	6	14	6	12
MCF sensor	17	20	15	14

the 200 °C–1000 °C calibrated range and the lower temperature sensitivity of the MCF below 100 °C as reported in [32].

For the results of the 25 °C-900 °C-25 °C loop shown in Fig. 8 only the curves of the packaged MCF sensor and the thermocouple are presented, since only the performance of these devices can be compared as their results are strictly related to temperature.

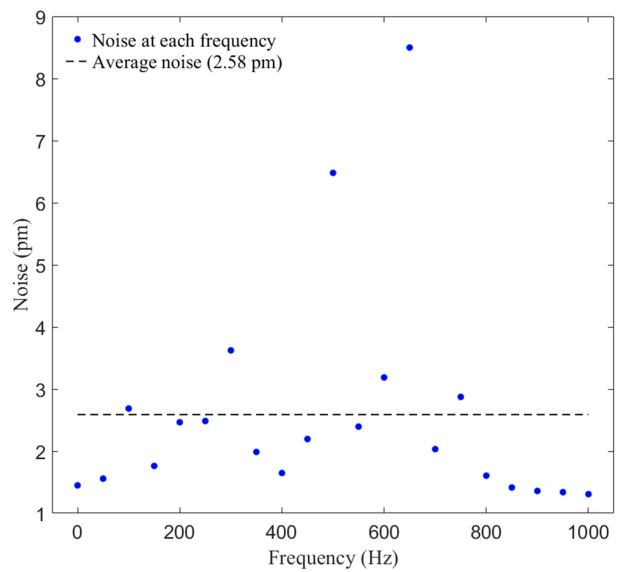


Fig. 9. Results of the effect of the vibrations in the measurements of λ_m at room temperature (25 °C). The biggest deviation (8.49 pm) happened at 650 Hz, where a resonance due to the 10 cm cantilever configuration took place.

The results shown in Fig. 7 and Fig. 8 are summarised in Table I. It can be noted that in all the cases, our packaged MCF temperature sensor responded slower than the thermocouple used as a reference. The results regarding the bare MCF are not shown in the table due to the fact that they are not related only to temperature, and therefore, not suitable for comparison.

In order to evaluate the effectiveness of the packaging in terms of protection against vibrations, the packaged MCF sensor was placed in a cantilever configuration and attached to a piezoelectric actuator (STr-35, Piezomechanik GmbH) whose maximum vibration amplitude was 6 μm . The length of the cantilever was 10 cm. The sensor was then subjected to vibrations at different frequencies. In all the cases, the voltage applied to the actuator

was the same (10 Vpp), and the measurements were carried out at room temperature (25 °C). The sensor was interrogated with the spectrum analyser mentioned above (I-MON512-USB, Ibsen Photonics) and the data processing approach was as follows: in two consecutive days 17000 raw spectra for each frequency were acquired and then, the maximum of each spectra (λ_m) was identified. These values were averaged for each point along with their standard deviation.

In Fig. 9, it can be seen that vibrations introduce an average noise of 2.58 pm in the measurement of λ_m . This turns into an uncertainty of 0.1 °C according to Eq. (2). Considering that the noise for the case of 0 Hz is intrinsic to the measurement system and not caused by vibrations, this means our MCF sensor is robust and practically immune to vibrations in a wide frequency range.

IV. CONCLUSIONS

In this work, we have reported on a sensitive and compactly packaged fiber optic temperature sensor that is robust against vibrations. The sensor is based on an MCF with strongly coupled cores. The sensor consists of a short segment of MCF (2.54 cm) spliced to a commonly used in telecommunications SMF. The fabrication of the device is simple, fast, inexpensive, and reproducible. The packaging of the sensor was conceived to make the MCF exclusively sensitive to temperature, hence independent to other parameters that may be present during temperature measurements, as for example, strain, bending, curvature, or vibrations.

The sensitive part of our sensor is the section of MCF. Temperature changes the effective indices of two supermodes that are excited in the MCF, causing a detectable shift in the interference pattern. The calibration of our MCF sensor was performed in the range from 200 to 1000 °C and a K-type thermocouple widely used and accepted in the conservative aeronautical industry was used as a reference. Results show that the packaged MCF sensor has a sensitivity of 24.8 pm/°C, high robustness against vibrations and a response time of 15 s. Thus, it may represent an attractive solution in several applications that require high temperature sensing, high resolution and sensitivity, small dimensions, and electromagnetic immunity. Some examples may include sensing in aeronautical engines, gas and oil facilities, etc.

The packaged MCF sensor can be customised for the aforementioned and other applications. In addition, its interrogation is carried out with commercially available sensor interrogators. Therefore, we believe that this prototype represents a substantial step forward in the direction of a commercially appealing optical temperature sensor.

REFERENCES

- [1] D. Bradley and K. J. Matthews, "Measurement of high gas temperatures with fine wire thermocouples," *J. Mech. Eng. Sci.*, vol. 10, no. 4, pp. 2328–305, Oct. 1968.
- [2] D. O'Sullivan and M. Cotterell, "Temperature measurement in single point turning," *J. Mater. Process. Technol.*, vol. 118, nos. 1–3, pp. 301–308, Dec. 2001.
- [3] M. Tagawa and Y. Ohta, "Two-thermocouple probe for fluctuating temperature measurement in combustion—Rational estimation of mean and fluctuating time constants," *Combustion Flame*, vol. 109, no. 4, pp. 549–560, Jun. 1997.
- [4] D. A. Stephenson, "Tool-work thermocouple temperature measurements—Theory and implementation issues," *J. Eng. Ind.*, vol. 115, no. 4, pp. 432–437, Nov. 1993.
- [5] L. Y. W. Lee, J. C. Chen, and R. A. Nelson, "Liquid-solid contact measurements using a surface thermocouple temperature probe in atmospheric pool boiling water," *Int. J. Heat Mass Transf.*, vol. 28, no. 8, pp. 1415–1423, Aug. 1985.
- [6] R. R. Dils, "High-temperature optical fiber thermometer," *J. Appl. Phys.*, vol. 54, no. 3, pp. 1198–1201, Nov. 1982.
- [7] V. Fericola and L. Crovini, "Digital optical fiber point sensor for high-temperature measurement," *J. Lightw. Technol.*, vol. 13, no. 7, pp. 1331–1334, Jul. 1995.
- [8] K. T. V. Grattan, A. W. Palmer, and Z. Zhang, "Development of a high-temperature fiber-optic thermometer probe using fluorescent decay," *Rev. Sci. Instrum.*, vol. 62, no. 5, pp. 1210–1213, May 1991.
- [9] Z. Zhang, K. T. V. Grattan, and A. W. Palmer, "Fiber-optic high-temperature sensor based on the fluorescence lifetime of alexandrite," *Rev. Sci. Instrum.*, vol. 63, no. 8, pp. 3869–3873, Apr. 1992.
- [10] G. Beheim, "Fiber-optic thermometer using semiconductor-etalon sensor," *Electron. Lett.*, vol. 22, no. 5, pp. 238–239, Feb. 1986.
- [11] M. Fokine and P. Holmberg, "Chemical composition gratings," presented at the OSA Tech. Dig. Adv. Photon. Conf., Barcelona, Spain, 2014, Paper SoW3B.4.
- [12] M. Fokine, "Formation of thermally stable chemical composition gratings in optical fibers," *J. Opt. Soc. Amer. B*, vol. 19, no. 8, pp. 1759–1765, 2002.
- [13] S. Bandyopadhyay, J. Canning, M. Stevenson, and K. Cook, "Ultra-high-temperature regenerated gratings in boron-codoped germanosilicate optical fiber using 193 nm," *Opt. Lett.*, vol. 33, no. 16, pp. 1917–1919, Aug. 2008.
- [14] S. Trpkovski *et al.*, "High-temperature-resistant chemical composition Bragg gratings in Er³⁺-doped optical fiber," *Opt. Lett.*, vol. 30, no. 6, pp. 607–609, Mar. 2005.
- [15] D. Barrera, V. Finazzi, J. Villatoro, S. Sales, and V. Pruneri, "Packaged optical sensors based on regenerated fiber Bragg gratings for high temperature applications," *IEEE Sensors J.*, vol. 12, no. 1, pp. 107–112, Jan. 2012.
- [16] S. S. Chong, W. Y. Chong, S. W. Harun, and H. Ahmad, "Regenerated fiber bragg grating fabricated on high germanium concentration photosensitive fiber for sensing at high temperature," *Opt. Laser Technol.*, vol. 44, no. 4, pp. 821–824, Jun. 2012.
- [17] S. J. Mihailov, "Fiber Bragg grating sensors for harsh environments," *Sensors*, vol. 12, no. 2, pp. 1898–1918, Feb. 2012.
- [18] S. Sales *et al.*, "Evaluation of new regenerated fiber Bragg grating high-temperature sensors in an ISO 834 fire test," *Fire Saf. J.*, vol. 71, pp. 332–339, Jan. 2015.
- [19] A. Wang *et al.*, "Sapphire-fiber-based intrinsic Fabry–Perot interferometer," *Opt. Lett.*, vol. 17, no. 14, pp. 1021–1023, Jul. 1992.
- [20] J. Wang *et al.*, "Multiplexed high temperature sensing with sapphire fiber air gap-based extrinsic Fabry–Perot interferometers," *Opt. Lett.*, vol. 35, no. 5, pp. 619–621, Mar. 2010.
- [21] Y. Zhu *et al.*, "Sapphire-fiber-based white-light interferometric sensor for high-temperature measurements," *Opt. Lett.*, vol. 30, no. 7, pp. 711–713, Apr. 2005.
- [22] C. Zhan *et al.*, "High temperature sensing using higher-order-mode rejected sapphire fiber gratings," *Opt. Memory Neural Netw.*, vol. 16, no. 4, pp. 204–210, Dec. 2007.
- [23] H. Y. Choi, K. S. Park, S. J. Park, U. C. Paek, B. H. Lee, and E. S. Choi, "Miniature fiber-optic high temperature sensor based on a hybrid structured Fabry–Perot interferometer," *Opt. Lett.*, vol. 33, no. 21, pp. 2455–2457, 2008.
- [24] T. Zhu *et al.*, "Fabry–Perot optical fiber tip sensor for high temperature measurement," *Opt. Commun.*, vol. 283, no. 19, pp. 3683–3685, Oct. 2010.
- [25] Y. Zhan *et al.*, "Fiber grating sensors for high-temperature measurement," *Opt. Laser Eng.*, vol. 46, no. 4, pp. 349–354, Jan. 2008.
- [26] V. M. Churikov, V. I. Kopp, and A. Z. Genack, "Chiral diffraction gratings in twisted microstructured fibers," *Opt. Lett.*, vol. 35, no. 3, pp. 342–344, 2010.
- [27] T. F. Morse, Y. He, and F. Luo, "An optical fiber sensor for the measurement of elevated temperatures," *IEICE Trans. Electron.*, vol. 83, no. 3, pp. 298–302, 2000.
- [28] G. Coviello *et al.*, "Thermally stabilized PCF-based sensor for temperature measurements up to 1000 °C," *Opt. Express*, vol. 17, no. 24, pp. 21551–21559, 2009.
- [29] D. Liu *et al.*, "Hollow core fiber based interferometer for high-temperature (1000 °C) measurement," *J. Lightw. Technol.*, vol. 36, no. 9, pp. 1583–1590, May 2018.

- [30] Z. Zhang *et al.*, "Hollow-core-fiber-based interferometer for high-temperature measurements," *IEEE Photon. J.*, vol. 9, no. 2, Apr. 2017, Art. no. 7101109.
- [31] T. Wang *et al.*, "A large range temperature sensor based on an angled fiber end," *Opt. Fiber Technol.*, vol. 45, pp. 19–23, Nov. 2018.
- [32] J. E. Antonio-Lopez *et al.*, "Multicore fiber sensor for high-temperature applications up to 1000 °C," *Opt. Lett.*, vol. 39, no. 15, pp. 4309–4312, Aug. 2014.
- [33] Y. Chunxia *et al.*, "Weakly-coupled multicore optical fiber taper-based high-temperature sensor," *Sens. Actuators A, Phys.*, vol. 280, pp. 139–144, Sep. 2018.
- [34] M. D. Wales *et al.*, "Multicore fiber temperature sensor with fast response times," *OSA Continuum*, vol. 1, no. 2, pp. 764–771, Oct. 2018.
- [35] J. Villatoro *et al.*, "Accurate strain sensing based on super-mode interference in strongly coupled multi-core optical fibers," *Sci. Rep.*, vol. 7, no. 1, pp. 4451–4457, Jun. 2017.
- [36] G. Salceda-Delgado *et al.*, "Compact fiber-optic curvature sensor based on super-mode interference in a seven-core fiber," *Opt. Lett.*, vol. 40, no. 7, pp. 1468–1471, Apr. 2015.
- [37] J. Villatoro *et al.*, "Miniature multicore optical fiber vibration sensor," *Opt. Lett.*, vol. 42, no. 10, pp. 2022–2025, May 2017.
- [38] J. Villatoro *et al.*, "Ultrasensitive vector bending sensor based on multicore optical fiber," *Opt. Lett.*, vol. 41, no. 4, pp. 832–835, 2016.
- [39] C. Xia *et al.*, "Supermodes for optical transmission," *Opt. Express*, vol. 19, no. 17, pp. 16653–16664, Aug. 2011.
- [40] C. Xia *et al.*, "Supermodes in coupled multi-core waveguide structures," *IEEE J. Sel. Topics Quantum Electron.*, vol. 22, no. 2, pp. 196–207, Mar.-Apr. 2008.
- [41] J. Taylor, "Uncertainty in the measurements of y ," in *An Introduction to Error Analysis: The Study of Uncertainties in Physical Measurements*, 2nd ed. Sausalito, CA, USA: Maple-Vail Book Manufacturing Group, 1997, pp. 186–188.
- [42] EGOLF (European Group of Organizations for Fire Testing, Inspection and Certification), Determination of the response time of thermocouples to be used for the measurement of air or gas phase temperature in reaction to fire testing, EGOLF Agreement EA 01: 2008, pp. 1–8, 2008.

Josu Amorebieta received the Master's degree in telecommunications engineering from the University of the Basque Country UPV/EHU, Bilbao, Spain, in 2016. He is currently working toward the Ph.D. degree with the Applied Photonics Group (APG-FAT), University of the Basque Country UPV/EHU. His current research interests include the optical fiber sensing utilizing special fibers for industry and aeronautics.

Gaizka Durana received the M.Sc. and Ph.D. degrees in solid-state physics and telecommunications engineering from the University of the Basque Country UPV/EHU, Bilbao, Spain, in 1999 and 2008, respectively. He is currently an Associate Professor with the Department of Communications Engineering, University of the Basque Country UPV/EHU. His research is focused on the manufacture of specialty polymer optical fibers and design, development, and application of fiber-based optical sensors.

Angel Ortega-Gomez received the Master's degree in telecommunications engineering from the University of the Malaga (UMA), Spain, in 2016. He is currently working toward the Ph.D. degree with the Applied Photonics Group (APG-FAT), University of the Basque Country UPV/EHU, Bilbao, Spain. His research is based on microstructure fibers sensors and Local Surface Plasmon Resonance (LSPR) effect applied on biosensors.

Rubén Fernández received the Electronics Engineer and Master's degrees in advanced electronics systems from the University of the Basque Country UPV/EHU, Bilbao, Spain. He is currently working toward the Ph.D. degree with the Applied Photonics Group (APG-FAT), University of the Basque Country UPV/EHU, Spain.

Javier Velasco is currently a Project Manager with the Aeronautical Technologies Center (CTA), Spain, and has been specialized during the last years in Industry 4.0. He has been working in several research projects focused on test control (load, vibration, and temperature), test automation, data acquisition, and monitoring technologies.

Idurre Sáez de Ocariz, biography not available at the time of publication.

Joseba Zubia, biography not available at the time of publication.

Jose Enrique Antonio-López, biography not available at the time of publication.

Axel Schülzgen received the Ph.D. degree in physics from Humboldt-University of Berlin, Germany. Since 2009, he has been a Professor of Optics and Photonics with CREOL, The College of Optics and Photonics, University of Central Florida, Orlando, FL, USA. He is also an Adjunct Research Professor with the College of Optical Sciences, University of Arizona, Tucson, AZ, USA.

Dr. Schülzgen has published more than 120 papers in peer-reviewed journals and holds six patents. He is a Fellow of the Optical Society of America.

Rodrigo Amezcua-Correa, biography not available at the time of publication.

Joel Villatoro received the M.Sc. and Ph.D. degrees in optics from the National Institute for Astrophysics, Optics, and Electronics, Mexico. He is an Ikerbasque Research Professor with the University of the Basque Country UPV/EHU, Bilbao, Spain. His research interests include optical fiber sensors and real-world applications of photonic technology.